Heim *et al. Geothermal Energy* (2024) 12:24
https://doi.org/10.1186/s40517-024-00303-8

Geothermal Energy

RESEARCH Open Access

Comparison of simulation tools for optimizing borehole heat exchanger field operation

Elisa Heim[1*], Phillip Stoffel[2], Stephan Düber[3], Dominique Knapp[4], Alexander Kümpel[2], Dirk Müller[2] and Norbert Klitzsch[1]

*Correspondence: elisa.heim@eonerc.rwth-aachen.de

[1] Computational Geoscience, Geothermics, and Reservoir Geophysics, RWTH Aachen University, Aachen, Germany
[2] Institute for Energy Efficient Buildings and Indoor Climate, E.ON Energy Research Centre, RWTH Aachen University, Aachen, Germany
[3] Geotechnical Engineering and Institute of Geomechanics and Underground Technology, RWTH Aachen University, Aachen, Germany
[4] Geophysica Beratungsgesellschaft mbH, Aachen, Germany

Abstract

Model predictive control (MPC) is a promising approach for optimizing the performance of borehole heat exchangers (BHEs) in ground-source heat pump systems. The central element of MPC is the forward model that predicts the thermal dynamics in the ground. In this work, we validate the prediction accuracy of four BHE modeling approaches against real-world measurement data across various operational events and timescales. We simulate the fluid temperature leaving a BHE using a fully discretized 3-D numerical model, a resistance–capacitance model, a g-function model, and a hybrid model. The simulated temperatures are compared to measured temperatures using three validation metrics that quantify temperature offset, noise, and accuracy. The main reason for a mismatch between measured and modeled temperatures is a temperature offset of the simulated temperature. To remove this effect, the models were calibrated for their most sensitive parameter, the ground temperature, and their prediction accuracy over 4 years was evaluated. Thereby, model calibration seems to be a viable solution to account for an unknown load history. The results show that the resistance–capacitance model provides decent predictions in the short term and the g-function model in the long term. However, both models are strongly dependent on accurate calibration. The hybrid model provides the most accurate short and long-term predictions and is less dependent on calibration. Still, its integration into optimization syntax poses challenges compared to the other models. Although not yet applied in model predictive control, the hybrid model stands out as a promising choice for optimizing BHE field operations across various timescales.

Introduction

Replacing fossil fuel-based heating systems with ground-source heat pumps (GSHPs) can significantly contribute to reducing the building sector's considerable carbon footprint. GSHPs rely on heat exchangers in the ground, which use the subsurface as a heat source in winter and heat sink in summer. The most common types of ground heat exchangers in Central Europe are borehole heat exchangers (BHE, Lund and Toth 2021). BHEs extract or inject heat into the subsurface using closed-loop pipes in vertical boreholes and are often composed of several BHEs, which is then referred to as BHE fields.

BHE fields must be designed to meet the load demand of a building over 30 to 50 years of operation. To achieve this, the design of BHEs is subject to various country-specific standards and regulations, for example the technical guideline VDI 4640 (2019) in Germany or the SIA 384/6 (2021) in Switzerland. All design approaches have in common that they require (1) an estimate of the building's energy demand, and (2) an estimate of in situ ground thermal properties. The buildings energy demand is usually calculated from the building type, usage and local climate, while ground thermal properties are derived from a thermal response test (TRT, e.g., Gehlin 2002). However, due to factors such as weather variability or occupancy changes, the actual energy demand of a building often deviates from the planned estimate (Bockelmann and Fisch 2019). Moreover, ground thermal properties are subject to uncertainty (Zhang et al. 2021), and the operation strategy can influence the thermal exchange processes in the subsurface (Shirazi and Bernier 2013). As a result, there tends to be a discrepancy between the anticipated and the real-world performance of GSHP systems. This so-called performance gap (de Wilde 2014) was recently emphasized in the GSHP context by several analyses of BHE field monitoring data (Spitler 2020; Bockelmann and Fisch 2019).

As building energy systems become more complex and BHE fields grow in size, recent research tries to tackle the performance gap to ensure long-term efficiency and sustainable operation (e.g., Soltan Mohammadi et al. 2024; Atam and Helsen 2016; Ma et al. 2020). One objective is to prevent a change in ground temperature in the long term, which usually causes a reduction of efficiency of the BHE field (e.g., Bayer et al. 2014; Liu et al. 2020) and thus an increase of operation cost in the long term. Another objective is to save operation costs in the short term, for example, by reducing the energy consumption of the hydraulic pumps moving the fluid in the pipes (Luo et al. 2017; Stoffel et al. 2022; Düber et al. 2024). For both objectives, operation optimization such as model predictive control (MPC) is becoming increasingly popular. In MPC, a predictive model is used to forecast future system behavior, and this prediction is employed to optimize the current set points of the system (Rawlings et al. 2017). The optimized operation can save both operation costs and ensure long-term efficient behavior (e.g., Ma et al. 2020; de Paly et al. 2012). For example, Verhelst et al. (2012) showed a 20–30% reduction of energy costs compared with standard control strategies, and Bayer et al. (2014) demonstrated an increase in long-term efficiency by limiting the change in ground temperature. Accordingly, MPC is expected to play an important role in the future operation of BHE fields by saving energy cost and sustaining long-term efficiency.

The central aspect of MPC is the process model that predicts the future energy output or fluid temperatures coming from the BHE field. Various BHE modeling approaches are available, which consider different heat transfer time and space scales (Li et al. 2014) and have been extensively reviewed (Yang et al. 2010; Bertagnolio et al. 2012). In general, four categories of BHE models can be distinguished. Fully discretized 3-D numerical models (1) can accurately simulate transient, 3-dimensional heat transport processes, but come with high computational effort. Simplified models are often based on the resistance–capacitance (RC) approach or thermal response functions/g-functions. Analogous to electric circuits, RC-models (2) model the GHE and/or the ground as a circuit of coupled thermal resistances and temperature nodes (e.g., Hellström 1991; Bauer et al. 2011; Zarrella et al. 2011; Pasquier and Marcotte 2012). G-functions (3) (Eskilson 1987)

describe the thermal response of a BHE in response to a unit step function and can be obtained from models (e.g., Cimmino and Bernier 2014; Pasquier et al. 2018) or from experimental data (Dion et al. 2022; Heim et al. 2024). Both RC and g-function models can focus either on the area inside the borehole, where rapid temperature changes occur due to the fluid circulation in the pipes, or the area outside the borehole (i.e., the soil/rock), which reacts dampened and with hysteresis to the heat exchange inside the borehole. Due to this differentiation, models are suitable for different time periods depending on their focus. Hybrid models (4) couple borehole and ground models to obtain the benefits of both categories (Düber et al. 2022; Mitchell and Spitler 2020). Available BHE models significantly differ in how they solve the thermal problem, depending on which area of the borehole they focus on, and which heat transfer processes they consider.

Recently, several models have been applied as predictive model for operation optimization. For example, Puttige et al. (2022) applied a hybrid analytical/neural-network model (Puttige et al. 2020b) to optimize the operation of a hospital building in Sweden, leading to a reduction of cost, CO_2 emission, and ground temperature change. Cupeiro Figueroa et al. (2020) employed a short-term BHE model to avoid heat-pump shutdown because of temperature limit constraints and saved 8.12% of costs. Models to be used within MPC must fulfill certain requirements, such as

- The predicted fluid temperature should be accurate, otherwise, derived control and optimization strategies will also not be optimal (Cupeiro Figueroa et al. 2021).
- The model should require minimal calibration and computational cost (Zhan and Chong 2021) and be implementable in simple hardware (Witte et al. 2018).
- The mathematical formulation of the model should allow for efficient optimization (linear, few states, no integer decisions, or twice continuously differentiable for nonlinear models).
- Ideally, the model keeps a certain physical significance (Zhan and Chong 2021), but a perfect process model is not required, especially not for short prediction horizons.

While operation optimization has promising potential for energy savings, to date, there is still uncertainty regarding which BHE model is best suited for MPC, considering these factors.

In this contribution, we validate four BHE models (one of each category) against high-frequency monitoring data of an operating BHE field. To this end, we simulate selected periods of operation with a numerical model, a g-function model, a RC-model and a hybrid model, both in calibrated and non-calibrated states. We evaluate the prediction accuracy of the models using three validation metrics and assert how much monitoring data the models require to make accurate predictions over a period of 4 years. Based on our results, we give recommendations for model selection for MPC.

Methods

In this section, we start by introducing the BHE field and the monitoring data. We then explain the four BHE models, which we compare by forward modeling and model calibration and then validate against experimental data.

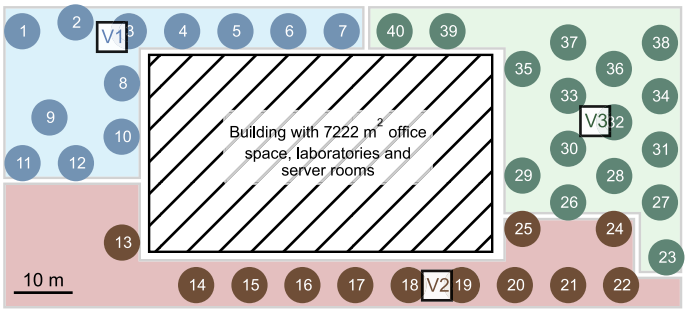

Fig. 1 Location of the 40 BHEs, assembled in three subfields (different colors), and underground vaults with sensors (marked with V1–V3). The circle size is not to scale

BHE field and monitoring data

The validation data come from the BHE field of the E.ON Energy Research Center (ERC), a research and demonstration facility with various energy sources, that is part of RWTH Aachen University (Germany). The BHE field comprises 40 double U-tube BHEs, each with a length of 100 m and linked to one of three underground vaults (Fig. 1). Inside the underground vaults, the pipes of the corresponding BHEs are assembled, thus dividing the field into three subfields. In the underground vaults, each BHE has a Belimo Energy Valve™ equipped with sensors for inlet and outlet fluid temperatures as well as volume flow. The temperature sensors of type PT1000 have a limit deviation of $\pm 0.3 + 0.005|T|$°C and were pairwise calibrated to reduce the measuring uncertainty. The measurements of the Belimo Valves are submitted in 30-s intervals to a monitoring system (Fütterer et al. 2013), which allows real-time data tracking and analysis of historical data. In addition, the Belimo Energy Valves™ serve as programmable logic controllers on which control algorithms can be implemented. As a result, the BHE field is well-equipped for implementing and testing operation strategies.

The BHE field has been in operation since November 2011, but due to the later installation of a monitoring system and database problems, the first trustworthy data were recorded in June 2014. However, even since then, some sensors have been out of operation or malfunctioning, such that the exact load history of the field is unknown.

Monitoring data

For the model comparison study, we chose two periods of 1 month each and a 4-year period from the monitoring data (Fig. 2). Because the temperature sensors are located in the underground vaults, data from BHEs close to the vaults were chosen (BHEs 17, 18 and 28, Fig. 1). This way, the temperature measurements are not influenced by the horizontal connecting pipe from the underground vault to the BHE head.

The 1-month periods are a heating period in winter and a cooling period in summer. The latter is a free cooling period (from mid-July to mid-August 2020), in which the heat pump was not operating and the geothermal field had to provide the entire building's cooling demand. An average inlet temperature of 17 °C resulted in a (for this BHE field) relatively high temperature difference (0.5 K to 1.5 K) between inflow and outflow (Fig. 2). The monitoring data show daily circulations of fluid temperature, while both inlet and outlet fluid temperatures increase by 1.5 K within

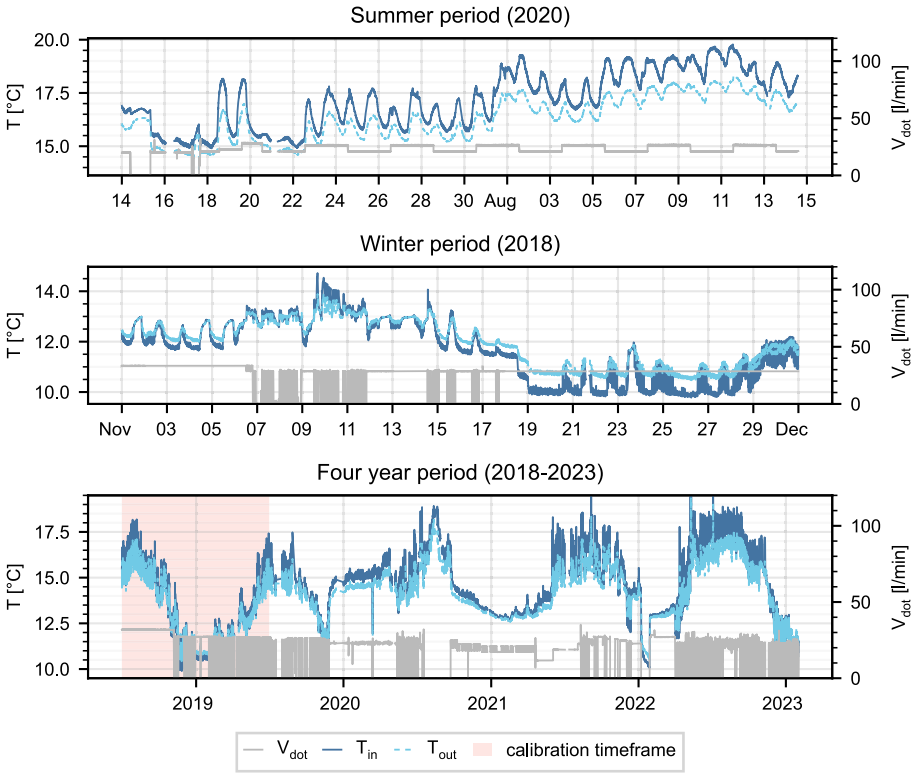

Fig. 2 Monitoring data used in this study. The summer (top) and winter (middle) period is used for the model comparison, and the 4-year period (bottom) for model calibration and comparison of the long-term prediction accuracy. The left axis shows the inlet and outlet temperature (T_{in}, T_{out}), and the right axis shows the volume flow (V_{dot})

the course of the month. In difference, the characteristic winter operation period of November 2018 shows an inlet temperature close to the ground temperature combined with an on–off operation of the hydraulic pumps. Even though the fluid was moved most of the time, the temperature difference between inflow and outflow does not exceed 0.5 K (Fig. 2).

The 4-year period from winter 2018 to spring 2023 combines several typical operation characteristics of the field: clocked operation with low temperature difference, as well as periods with a higher heat exchange rate. Both inflow and outflow temperatures follow the yearly sinusoidal temperature variation, with higher temperatures in summer and colder temperatures in winter.

The monitoring system records the temperature and volume flow data of each BHE in 30-s intervals, which are further downsampled (via averaging) to 5-min and 1-h intervals. All three time resolutions (30 s, 5 min, and 1 h) are used to analyze their influence on the prediction accuracy of the models.

Table 1 BHE and ground properties of the EON.ERC field

Parameter	Value	Units
Fluid properties		
Thermal conductivity	0.43	$W\,m^{-1}K^{-1}$
Density	1054	$kg\,m^{-3}$
Volumetric heat capacity	3,800,000	$J\,m^{-3}K^{-1}$
Dynamic viscosity	0.0035	Pa s
BHE geometry		
Length	100	m
Borehole diameter	0.152	m
Horizontal pipe distance	0.04	m
Pipe outer diameter	0.032	m
Pipe wall thickness	0.0029	m
BHE material properties		
Grout thermal conductivity	2.0	$W\,m^{-1}K^{-1}$
Grout volumetric heat capacity	1,000,000	$J\,m^{-3}K^{-1}$
Pipe thermal conductivity	0.3	$W\,m^{-1}K^{-1}$
Ground properties		
Average thermal conductivity	2.3	$W\,m^{-1}K^{-1}$
Average volumetric heat capacity	2,300,000	$J\,m^{-3}K^{-1}$
Initial ground temperature	12.0	°C

Models and their parametrization

Four models are used to simulate the outlet temperature of a BHE—a fully discretized numerical model, a g-function model, a RC-model, and a hybrid model. All models consider only heat conduction in the ground. The models are briefly described in the following. For details regarding the implementation, we refer to the original publications. All models are parameterized with the same technical and thermal properties of the BHE field, that are summarized in Table 1.

Numerical model

To provide a fully discretized numerical underground model, we use the open-source software SHEMAT-Suite (Keller et al. 2020). In SHEMAT-Suite, the underground model can be coupled to two different nested model implementations of a BHE. Here, we use an explicit semi-analytical thermal resistance–capacitance formulation as the BHE model. To couple the explicit BHE model to the numerical underground model, a volumetric sink and source term as interface for heat production and extraction in distinct BHE cells (Mottaghy and Dijkshoorn 2012) is used. The second interface between the models is the borehole wall temperature. This temperature is extracted from the underground cells surrounding the discrete BHE cells and serves as a borehole wall temperature boundary condition for the explicit BHE model in the corresponding extraction time step. In contrast to Mottaghy and Dijkshoorn (2012), we use the resistance–capacitance model presented in Bauer et al. (2011) to calculate the horizontal heat flow from the surrounding underground cells to the BHE. This is achieved based on the difference between the inlet and outlet fluid temperatures as well as the borehole wall temperature.

The fluid temperature along the BHE pipes is calculated at time and depth using an explicit forward scheme, and the calculated heat flux is returned to the underground model as a volumetric source term along the pipe length. As a consequence of the heat exchange, the borehole wall temperature is updated and serves as a new boundary condition for the next explicit time step. This model formulation is similar to the one used in common BHE simulation software codes.

G-function model

The g-function model used in this study refers to the temperature response factor model implementation available in the Python package *pygfunction* (Cimmino 2018). The area inside the borehole is represented by an analytical thermal resistance model derived from the steady-state heat transfer equation (Cimmino 2016). To assess borehole thermal resistances, the multipole method (Claesson and Hellström 2011) is used. The analytical borehole model is coupled to a finite line source model (Cimmino and Bernier 2014) representing the ground using the borehole wall temperature as interface. For the calculations of individual BHEs, the borehole wall temperature is assumed to be uniform along the entire BHE length.

G-functions are commonly used for designing BHE fields based on thermal loads. This approach requires some simplifying assumptions for simulating operation data: instead of the inlet temperature, the model takes as input a heat extraction rate $\dot{Q}$ to predict the outlet fluid temperature, which is calculated from the monitoring data as:

$$\dot{Q} = c_\mathrm{f}\rho_\mathrm{f}\dot{V}\left(\dot{T}_\mathrm{out} - \dot{T}_\mathrm{in}\right), \tag{1}$$

where c_f and ρ_f are the volumetric heat capacity and the density of the fluid, $\dot{V}$ the volumetric flow rate, and $\dot{T}_\mathrm{in}$ and $\dot{T}_\mathrm{out}$ the inlet and outlet fluid temperature. The calculation of the g-function is independent of the fluid flow rate, but the flow rate is needed for the calculation of the fluid temperature. The in *pygfunction* implemented model assumes a constant flow rate, which is calculated here by averaging the measured fluid flow rate for the respective simulation period. This simplification is reasonable, since the dependence of the g-function on the mass flow rate is negligible for parallel-connected boreholes, as long as the mass flow is sufficiently high (Cimmino 2019, 2015).

By definition, the g-function model is only valid for steady-state heat transfer conditions where, according to Eskilson (1987), $t \geq 5r_\mathrm{b}^2/\alpha_\mathrm{s}$ (Cimmino 2016). This is the time it takes for a heat pulse to reach the borehole wall (Shirazi and Bernier 2013), and is around 8 h for the BHEs of this study. Thus, the model is theory-wise not qualified to simulate the operation of a BHE field with frequently changing fluid flow rates and inlet temperatures, which is the case at the studied BHE field.

Hybrid model

The hybrid model presented by Düber et al. (2022) follows the idea of Wetter and Huber (1997) of combining a semi-numerical borehole model with a g-function ground model. Similar to the numerical model, the borehole model utilizes a vertically discretized resistance–capacitance approach (Bauer et al. 2011) for the horizontal heat transfer and the finite volume method for the heat transfer in the vertical direction. The heat transfer in the ground is modeled with a combination of analytically determined g-functions to

cover a time range from seconds to decades (infinite cylinder source, infinite line source and finite line source, Li et al. 2014). Similar to the g-function model, the consideration of time-variable loads is taken into account by temporal superposition. To overcome high computational times for simulations with many time steps, the model employs the fast Fourier transformation and the convolution theorem for better efficiency (Marcotte and Pasquier 2008).

The hybrid model uses the measured inlet temperature and fluid flow rate to calculate the outlet temperature. In Düber et al. (2022), the model was verified with both numerical simulations and monitoring data.

Resistance–capacitance (RC) model

The simplest physical model used was presented by Stoffel et al. (2022) and is solely based on a resistance–capacitance approach. It describes the thermal behavior by lumped capacities with different temperatures in three discrete shells of different diameters surrounding the borehole, and thermal resistances in between. The model determines the outlet temperature of a single BHE by the heat transfer between the fluid and the borehole wall, taking into account the other shell temperatures. Thereby, the first shell represents the borehole, and the second and third layers the soil. The soil temperature around the third layer is assumed to be constant and equal to the ground temperature (Table 1).

The model uses the measured volume flow rate and the inlet temperature to compute the temperatures in the three shells, as well as the fluid outlet temperature. An advantage of this model, compared to the other approaches, is that it can easily account for operation history by adjusting the temperatures in the three shells. The model was designed for short time scales up to 1 month, as it does not consider thermal interaction between the pipe legs, and is only valid for turbulent flow.

Model calibration and assessment of required calibration period

Sensitivity study

To analyze which model parameter should be calibrated, we studied the sensitivity of the models to five subsurface parameters. The methodology is based on Fernández et al. (2017). The authors applied sensitivity analysis to a model of a borehole field with six BHEs and analyzed the impact of 20 parameters on both the fluid temperature and the heat transfer rate. From the results, they conclude that of in total 20 parameters, only five are relevant and should be calibrated for BHE models: the flow rate, the initial temperature, the specific heat capacity of the fluid, and the thermal conductivity of both ground and grout.

Here, we know the flow rate from the monitoring data and the fluid properties from the manufacturer. For this reason, we analyze the sensitivity of the models towards the remaining subsurface and grout parameters. Assuming that the subsurface properties are not precisely known, parameter ranges (Table 2) were assigned to be within ±20% of the initial parameters given in Table 1.

Based on the parameter ranges, we analyze the Sobol sensitivity using the python library SALib (Iwanaga et al. 2022; Herman and Usher 2017) with the Saltelli sampler (Saltelli 2002; Saltelli et al. 2010). The Sobol method is a variance-based sensitivity

Table 2 Parameter ranges considered in the sensitivity study

Parameter	Min	Max	Unit
Ground temperature	10	14	°C
Ground thermal conductivity	2.1	2.7	W/(mK)
Grout thermal conductivity	1.7	2.3	W/(mK)
Ground specific heat capacity	1.9	2.6	$MJ/m^3/K$
Grout specific heat capacity	0.8	1.4	$MJ/m^3/K$

analysis method; it decomposes the variance of the output into contributions from the individual input parameters. The total-order Sobol index provides the sensitivity of the output towards changes in the input parameters, including parameter interactions. It is calculated for each parameter at each timestep for both the summer and winter periods, to see how the sensitivity index changes with time.

Calibration

Based on the results of the sensitivity study, the models are calibrated for their most sensitive parameter, the ground temperature T_0. For calibration, we minimize the difference between measured and simulated temperatures by optimizing the calibration parameter using the Python package *scipy.optimize* (Virtanen et al. 2020). Thereof, the "brute" function is used, with a T_0 parameter range between 10 and 14 °C, and an initial guess of 12 °C.

In addition to calibrating the models for the entire period, we assess how much data are required to obtain a stable estimate of T_0. For analyzing the necessary length of the calibration period, we calibrate the models with different periods of monitoring data. The calibration is done for each model for 18 periods, ranging from 1 day to 1 year: 1, 1.5, 2, 3, 5, 7, 11, 25, 38, 57, 86, 129, 176, 223, 270, 317 and 364 days. The analysis is conducted for all three data resolutions (30 s, 5 min, and 1 h) to see if the resolution affects the calibration results.

Model validation and comparison

The simulated outlet fluid temperatures predicted by the models are compared to the measured fluid temperatures both qualitatively (by visual comparison) and quantitatively using three validation metrics, the mean absolute error (MAE), the centered mean squared error (CMSE), and the Nash–Sutcliffe efficiency (NSE). The MAE is a standard approach for quantifying the mismatch between measured and modeled data. It is calculated from the measured time series y_t and modeled time series $\hat{y}_t$ as

$$\mathrm{MAE} = \frac{\sum_{t=1}^{n} |y_t - \hat{y_t}|}{n}. \tag{2}$$

However, the MAE does not allow distinguishing between an offset in time (x) or temperature (y) direction. We want to predict if the models can recreate the general trend (the shape) of the temperature evolution and thus neglect the temperature offset. For this, we use the CMSE, which is calculated as:

$$\mathrm{CMSE} = \frac{1}{n-1}\sum_{t=1}^{n}\left(y_t - \hat{y}_t - \mathrm{mean}(y_t - \hat{y}_t)\right)^2. \tag{3}$$

In addition, we want to disregard noise, due to sensor inaccuracies, when comparing the modeled and measured temperatures. For that, we compute the NSE (Nash and Sutcliffe 1970), which punishes a shift in time, a different amplitude, and compression of the temperature, but gives less weight to small-scale variations (i.e., noise). It is calculated by subtracting the ratio of the variance of the modeled temperature and the variance of the measured temperature from one:

$$\mathrm{NSE} = 1 - \frac{\sum_{t=1}^{n}\left(y_t - \hat{y}_t\right)^2}{\sum_{t=1}^{n}\left(y_t - \bar{y}\right)^2}, \tag{4}$$

with $\bar{y}$ as the mean observed temperature over the considered time period. The NSE is a similarity measure instead of an error measure. If two time series perfectly lie on top of each other, the NSE is one, and the less similar the time series are, the closer it is to zero. Values below zero indicate that the mean of the measured data is a better indicator than the modeled data, i.e., the error variance of the modeled data exceeds the variance of the measured data.

Results

We first show the results of the sensitivity study, on which the model calibration is based on. Next, for model comparison, we present three studies comprising forward modeling, model calibration, and validation against experimental data. The studies are summarized in the following.

1. Short-term prediction accuracy: The models are implemented with the same constant parameters (Table 1), and simulate the characteristic heating and cooling period of one month each (Fig. 2). Then, the modeled temperature is validated against the experimental temperature using the three error metrics. Subsequently, the models are calibrated and the reduction in error metrics is analyzed.
2. Assessment of required calibration period: We investigate how the length of the calibration period (and time resolution) influences model calibration ("Model calibration and assessment of required calibration period" section).
3. Long-term prediction accuracy: The prediction accuracy of the models over 4 years is compared. For this, each model simulates data of 4 years, both for non-calibrated conditions and for calibration parameters obtained from the respective model calibration of step 2.

Before presenting the results of the studies, the computation time of the models is compared. On a standard laptop with an i7-11850 H processor (4.8 GHz), the calculation of 105120 time steps took 4.8 s for the g-function model, 21 s for the hybrid model, 84 s for the RC model and around 12 days for the numerical model.

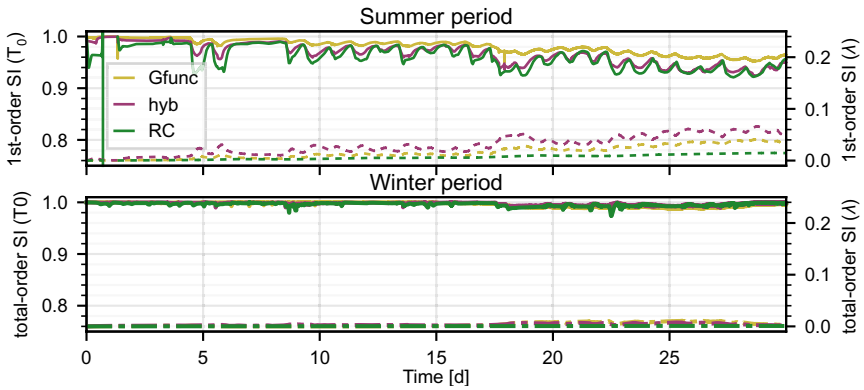

Fig. 3 Total sensitivity indices (SI) of the three models for the summer period (top) and winter period (bottom) to T_0 (solid lines, left axis) and the thermal conductivity of the ground λ (dashed lines, right axis). Note the different scaling of the sensitivity axes. RC: resistance–capacitance model; Hyb: hybrid model; Gfunc: G-function model

Sensitivity study

The sensitivity study shows that the outlet temperature of the g-function, hybrid and RC models has the highest sensitivity to T_0. Analyzing the sensitivity of the numerical model was not feasible due to its high computation time. Figure 3 shows the total Sobol index (SI) of the ground temperature (T_0, left axis) and the thermal conductivity of the ground (λ, right axis) at each timestep for the summer and winter period. In both periods and for all models, the contribution of T_0 is constantly higher than 0.9. The second most sensitive parameter is the ground thermal conductivity, whose sensitivity increases with time but generally remains below 0.1. The sensitivity towards the other investigated parameters, as well as parameter interactions, are negligible and thus not shown. As all models are most sensitive to T_0, this parameter was chosen for model calibration.

Short-term prediction accuracy

The characteristic summer and winter operation periods is simulated with all models, first with the same assumed T_0 of 12 °C, and later for models with a calibrated T_0. The results are presented in the following.

Uncalibrated models

Summer period The weekly averaged error metrics between the measured and modeled temperatures for the summer period are shown in Fig. 4 (top left). All error metrics show that all models have their highest deviation to the measured temperature at the beginning. After 1 week, the numerical and hybrid models have absolute errors of less than 0.1 K with neither temperature offset (low CMSE) nor different shape (high NSE). The outlet temperature calculated by the RC model is offset from the measured temperature, indicated by a zero CMSE, but an average NSE of 0.5 and a MAE of 0.2 K. This offset from the measured temperature is even more pronounced for the g-function model with an MAE higher than 2 K (Fig. 4).

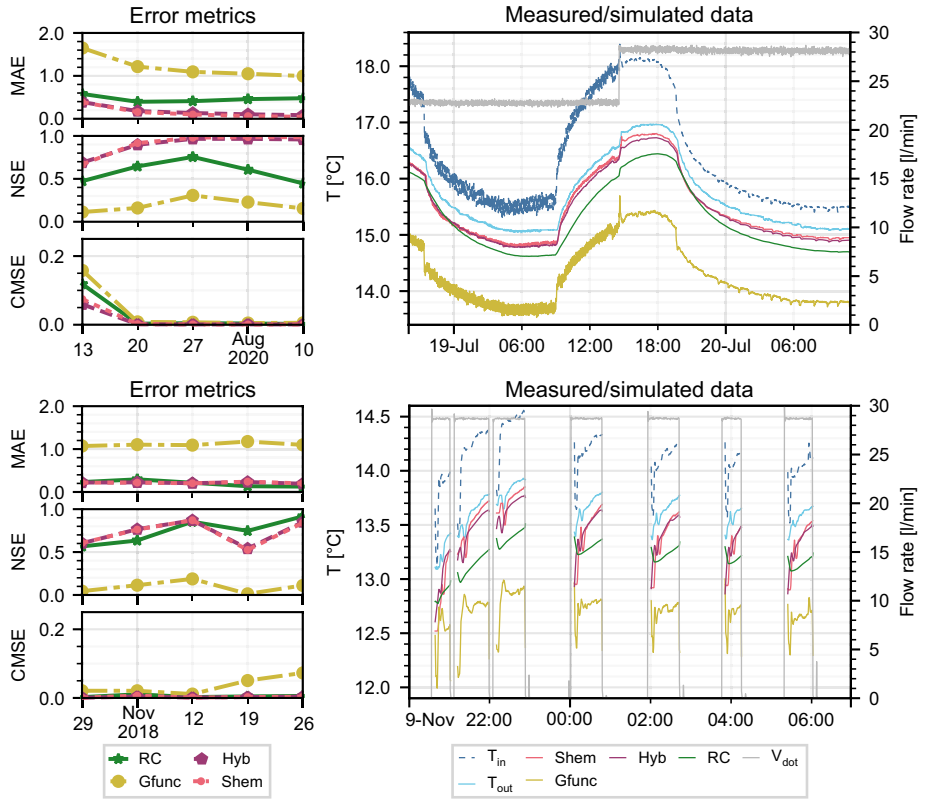

Fig. 4 Data and model comparison for the summer (top row) and winter period (bottom row) for uncalibrated models. Weekly average of the errors (left column) and zoom on short periods (40 h and 10 h) of the measured and simulated outlet temperatures (right column). RC: resistance–capacitance model; Hyb: hybrid model; Gfunc: G-function model; Shem: numerical model; T_{in}: measured inlet temperature; T_{out}: measured outlet temperature; V_{dot}: measured volume flow

Figure 4 additionally shows a short period of absolute measured and modeled temperatures, which shows how the models react to a change in flow rate. Both the numerical and hybrid models reproduce the increasing outlet temperature well. The RC model reproduces the temperature increase in a damped manner, while the g-function model, using the monthly average flow rate, does not show an increase.

Winter period Different to the summer period, the error metrics are mostly consistent over time. Again, the numerical and hybrid model reproduce the measured temperature best, but their NSE is slightly lower than in the summer period (Fig. 4, bottom left). The performance of the RC model is comparable to the numerical and hybrid models. The g-function model performs poorly in this period, with an NSE approaching zero, suggesting that using the mean of the measured data would yield a better prediction than relying on the model.

Figure 4 (bottom right) shows the absolute temperatures for a short-clocked operation phase. The numerical and hybrid model underestimate the measured temperature, which is a likely explanation for the slightly lower NSE than in the summer period. Moreover, the rate of temperature increase during circulation differs. For the numerical, RC, and hybrid models, it corresponds to the rate of temperature increase

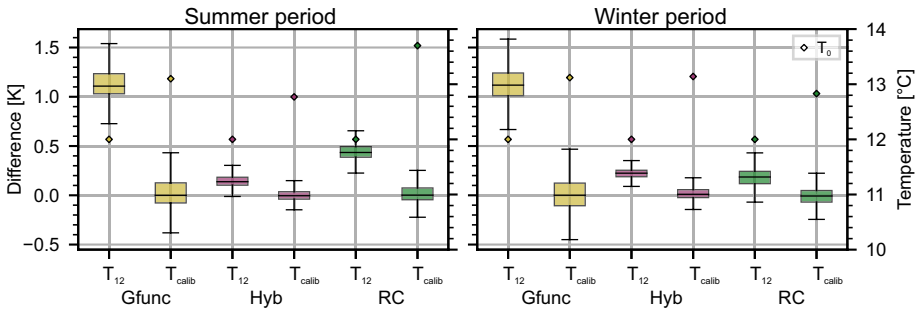

Fig. 5 Difference between the measured and simulated data for uncalibrated (T_{12}) and calibrated (T_{calib}) model predictions for the summer (left) and winter period (right). The diamonds belong to the right axis and show the T_0 used for the simulation, which is either 12 degrees (T_{12}) or the temperature obtained from the calibration (T_{calib})

in the measured data. The g-function model exhibits a lower slope compared to the measured temperature, presumably caused by the neglected heat capacity of the borehole (Shirazi and Bernier 2013).

Calibrated models

Summarizing the observations of the model predictions in an uncalibrated state, the hybrid and numerical models show a similarly accurate prediction accuracy for both the summer and winter period. However, the numerical model requires significantly more computation time. For this reason, the numerical model is not included in further investigations. The RC model reproduces the measured temperature in a damped manner and partly has a temperature offset. The g-function model has difficulties in predicting the correct temperature, especially for the winter period with clocked operation phases, which is not surprising considering the formulation with a ground load. For the summer period, the main error is a temperature offset to the measured temperature, which can be removed by model calibration.

After calibrating the models for T_0, the prediction accuracy of the g-function and RC model increases substantially. Figure 5 shows the difference between measured and simulated data (residuals) over the entire summer and winter period for models with $T_0 = 12$ °C (not calibrated) and models with calibrated T_0. In the figure, the box height ranges from the first to the third quartile; the horizontal line inside the box corresponds to the median. The whiskers visualize the highest residual inside 1.5 times the interquartile range. The figure shows that the prediction accuracy of all models benefits from the calibration, with the median residual being reduced to zero. However, the interquartile range (box in Fig. 5) and the whisker length are not influenced by model calibration.

Figure 5 also shows that the T_0 obtained from the calibration is different for the models. It ranges between 12.8 and 13.7 °C for the summer period, and 12.8 °C and 13.1 °C for the winter period.

Length of the calibration period

The calibration for a data period of 1 month has shown that the models return different T_0. To investigate if T_0 is influenced by the length of the data period, we calibrate the models with different lengths of calibration periods for the three models and time

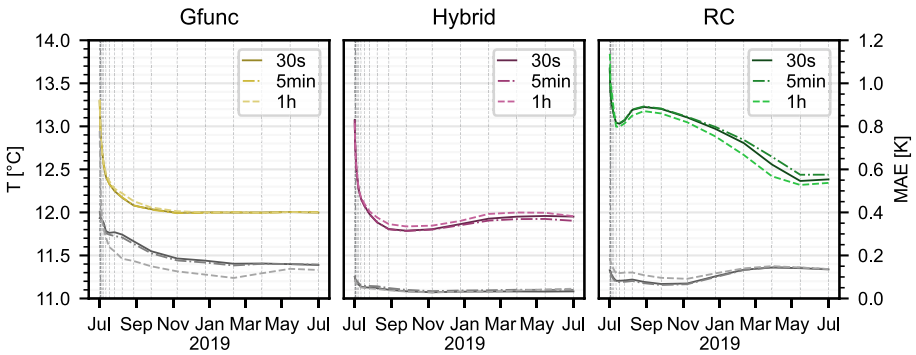

Fig. 6 Estimated T_0 (left axis) in dependence of the calibration period (gray vertical lines) for different measurement resolutions (30 s, 5 min and 1 h). The gray lines show the mean absolute error (MAE) of the estimated temperature (right axis)

resolutions (300 s, 5 min, and 1 h, Fig. 6). In addition to the estimated T_0, the figure shows the corresponding MAE (gray lines). For all models and all time steps, T_0 is overestimated with short calibration periods. This observation is in accordance with the initial underestimation of the fluid temperature for the summer period ("Uncalibrated models" section). With calibration periods of more than three or six months, both the g-function and hybrid model, respectively, tend to settle towards a T_0 of 12 °C. The RC model reaches a temperature of 12.5 °C with the full 12-month calibration period, but it does not seem to settle on this value. Comparing the hybrid and the g-function results, it is interesting to note that T_0 estimated with the hybrid model first shows a downward deflection to 11.8 °C (Fig. 6). The timestep slightly influences the exact value of T_0 for the hybrid and RC models; for the g-function model, the timestep does not affect the estimate. The MAE of the g-function model decreases with increasing timestep, i.e., coming closer to the timestep required to fulfill the steady-state assumption. However, no significant reduction of the estimation error is obtained when doing the calibration with a timestep of 8 h (which corresponds to the time required to fulfill the steady-state assumption).

Long-term prediction accuracy

The optimized temperatures obtained from the model calibration with 12 months of monitoring data were used to model the remaining operation period of BHE 18 until the end of January 2023 (4 years). In addition, based on the model calibration results of the 1-month period, all models were run with a starting temperature of 12.8 °C, i.e., with the same assumed temperature, and a data resolution of 30 s. The temperature was chosen based on the calibration results of the short period, which indicated that T_0 is higher than 12 °C (Fig. 5). The residuals between the measured and simulated temperatures of the calibrated models is shown in Fig. 7 (left) and the box–whisker plot for the entire period for calibrated and uncalibrated models in Fig. 7 (right).

While the g-function and hybrid model benefit from the calibration (the median deviation is reduced from 0.8 K to zero for the g-function model and from 0.18 K to 0.02 for the hybrid model), the calibrated RC-model performs worse compared to the uncalibrated model. This is not surprising, as the RC-model did not settle on a constant temperature in the assessment of the length of the calibration period, resulting in the

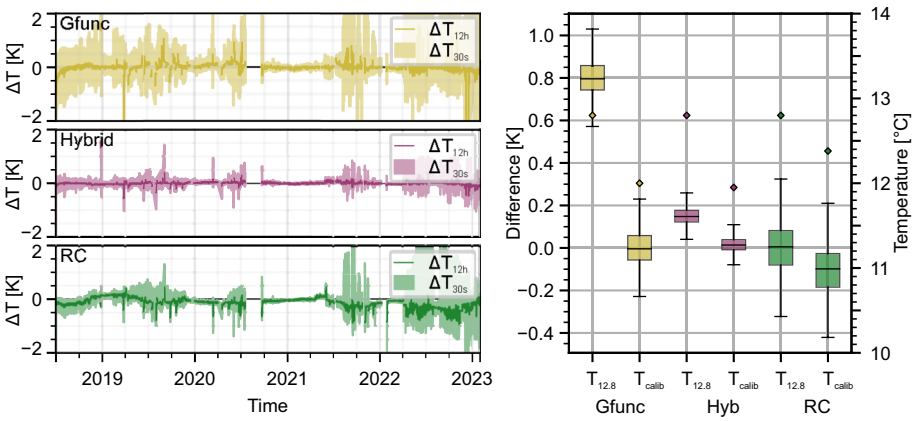

Fig. 7 Difference between simulated and measured data with calibrated temperatures for 4 years (left) and box–whisker plot for calibrated and uncalibrated temperatures (right). The lines in the whisker plot show the median residual over the 4-year period

assumption of 12.8 °C being a better choice. Similar to the 1-month data periods, the calibrated hybrid model has the highest accuracy, with a median close to 0 and an interquartile range of 0.1 K. The calibrated g-function model has its median also at zero, but the interquartile range is higher (0.3 K). This can also be seen in the plot on the left-hand side, with a difference ranging between −2 and 2 K. Similar to the observations made for the monthly comparison, all models show the highest deviation to the measured temperature during cyclic operation phases, i.e., when the volume flow changes rapidly (on-off operation, compare Fig. 4). Over 4 years, the mean absolute error of the calibrated g-function model is 0.11 K, of the RC model 0.15 K and of the hybrid model 0.03 K, i.e., all models have on average a high prediction accuracy.

Discussion

Here, we first summarize and discuss the results concerning the four MPC requirements outlined in the introduction. Based on this, we provide recommendations for model selection for MPC. Next, we present two examples of successful applications of MPC using RC and g-function models. We continue with a more detailed discussion of the calibration for an unknown load history, as well as problems with the predictive accuracy of the models for specific BHE operations.

Model selection

To give a recommendation for model selection, we summarize and discuss the results in hindsight of the four aspects that were pointed out in the introduction, namely the

- accuracy of the predicted fluid temperature,
- physical significance of the models,
- optimizability of the models in terms of the mathematical formulation, and
- calibration requirement and computational cost.

Table 3 Statistics of the temperature difference (median and interquartile range, in Kelvin) between simulated and measured data periods for uncalibrated and calibrated (in italics) g-function, hybrid, and RC models

	Summer			Winter			4 years		
	T_0 [°C]	Median	Range	T_0 [°C]	Median	Range	T_0 [°C]	Median	Range
Gfunc	12	1.11	0.2	12	1.13	0.22	12.8	0.8	0.11
	13.11	*0*	*0.2*	*13.12*	*0.01*	*0.22*	*12*	*0*	*0.11*
Hyb	12	0.14	0.08	12	0.22	0.06	12.8	0.15	0.05
	12.77	*0*	*0.08*	*13.14*	*0.02*	*0.08*	*11.95*	*0.01*	*0.05*
RC	12	0.43	0.11	12	0.19	0.11	12.8	0.01	0.16
	13.7	*0*	*0.12*	*12.83*	*0*	*0.11*	*12.38*	*−0.1*	*0.16*

Accuracy of predicted fluid temperature

The hybrid model demonstrates the ability to predict the measured outlet temperature with the highest accuracy across all scenarios, both in calibrated and uncalibrated states. This level of accuracy is comparable to that of the numerical model, yet the hybrid model achieves it in significantly less computational time (10^5 times faster). When calibrated, the median temperature deviation of the hybrid model is zero, with an interquartile range as low as 0.05 (see Table 3). Even though calibrating the RC and g-function model also reduces their median deviation to zero for the summer and winter periods, their interquartile range is not smaller than 0.11.

Physical significance

The simplifications made to speed up the models and their focus on different timescales are observable in the predicted fluid temperature, especially in their interquartile range (Table 3). The physical significance of the models differs, with the RC model having the most simplifications, followed by the g-function and hybrid models. The numerical model represents the actual physics most realistically. This is reflected in how the models reproduce the fluid temperature: despite calibration, the RC model, tailored for short simulation periods, dampens the outlet temperature and cannot predict long-term performance. The outlet temperature of the g-function model, designed for long-term predictions, has a different shape than the measured data due to its formulation with a ground load. The hybrid and numerical models integrate heat transfer processes both inside and outside the borehole. Thus, their outlet temperatures closely align with the monitoring data.

Optimizability (mathematical formulation)

Besides the prediction accuracy and the physical significance, models must fulfill additional requirements to be successfully implemented in MPC. Particularly, optimization ability and computational efficiency are highly relevant. The numerical model with its high computation time is thus unsuitable for MPC. Although the hybrid model is less complex than the numerical model, it incorporates more nodes for discretizing the ground compared to the RC and g-function models. For application in MPC, these additional nodes increase the computational effort, and a reformulation in optimization syntax [(for example, by using CasADi (Andersson et al. 2019)] would be required. The RC

and the g-function models have a reasonable complexity; both models allow the formulation of linear or weakly nonlinear optimization problems. To illustrate model applications, we showcase how the g-function and RC models were used to improve the BHE field control of the E.ON ERC building in the "Applications of BHE models for MPC" section.

Calibration requirement and computational cost

The average deviation from the measured outlet temperature for both summer and winter periods of all models is reduced to zero by calibration. Even when not calibrated, the hybrid model is still closest to the measurements, with a median deviation of 0.22 K for the winter period (Table 3), thus having the lowest calibration requirement. The g-function model suffers most from a lack of calibration, showing a temperature offset of up to 1.13 K to the measured temperature (Table 3).

However, our analysis reveals that for long-term predictions, both the hybrid and g-function models demonstrate accurate forecasting of the outlet temperature over four years once T_0 stabilizes over an increasing length of the calibration period. Both models converge to the same value of T_0, but the g-function model achieves stability with just three months of monitoring data compared to the hybrid model's requirement of six months. Moreover, the g-function model's calibration result is independent of the data's time resolution. The g-function model in a coarse time resolution, combined with its short computation time, appears well-suited for parameter estimation. The parameters could subsequently inform the forward simulations using the hybrid model. Further exploration of this aspect will be conducted in detail in the section "Calibration to account for unknown load history".

The RC model did not reach a stable calibration temperature. However, because of its different formulation, the RC model can be used as an online model for n-steps-ahead predictions, with the temperatures of the three shells being calibrated independently. An example of this approach is given in the section "Applications of BHE models for MPC".

Summary: recommendations for model selection

To summarize, the hybrid model by Düber et al. (2022) seems to be the perfect choice to fast and efficiently predict the outlet temperature of BHEs for both short and long timescales. Its formulation can also account for thermal interaction between multiple BHEs, and the code is publicly available via GitHub.[1] However, even though the hybrid model has the lowest calibration requirement, the g-function model was (in this study) the most efficient for finding the calibration parameter. Both the g-function and RC models fulfill other requirements of MPC towards BHE models. Provided that the physical simplifications affecting their application purpose are taken into account, both models are suited to be used in MPC, and we present two applications of the models to improve the BHE field operation in the following section.

[1] https://github.com/GUT-Aachen/Hybrid-BHE-Simulation-Model.

Applications of BHE models for MPC

Here, we present two use cases that apply the g-function and RC models for optimizing the operation of a building's energy system and its BHE field.

Long-term optimization using the g-function model

Optimization studies using g-function models usually optimize how the load is distributed over various energy sources over several years. Kümpel et al. (2022) use a g-function model to represent the subsurface heat exchange while optimizing the long-term operation of the ERC's energy system. In their approach, each component of the building (heat pump, two boilers, a combined heat and power system, air-handling units, concrete core activation, and BHE field) is represented as a sub-model, connected via heat flow rates to form the overall energy system. The energy system's operation is optimized for a period of 15 years using a mixed-integer linear program. The optimization returns the heat flow rates produced or consumed by the components and the ground temperature, and was solved by minimizing energy cost, the change in ground temperature, or both jointly (multi-objective optimization). The results show that in the temperature-based optimization, the change in ground temperature can be reduced to nearly zero at the end of the optimization period. In the case of the cost-based optimization, the ground temperature increases asymptotically but remains below 2.1 K at the end of the studied 15-year period. In the multi-objective optimization, the cost increased by 1%, but the ground temperature remained constant.

The authors highlight that due to its fast computation time, the g-function model is well-suited for load-balancing optimization over several years. Another advantage is that the approach leads to a linear system of equations if the g-function is calculated a priori. Similar studies optimizing long-term performance were conducted by other authors (Puttige et al. 2022; Bayer et al. 2014). The results of such studies are impressive in terms of theoretical energy savings, but, to our knowledge, so far only based on simulations—validation with actual data is yet to be done. Here, our results from the model calibration study could help deciding on the necessary data period for model calibration, before starting the actual optimization.

Short-term optimization using a RC model

The RC model is implemented in a MPC for the E.ON ERC building's short-term optimization, demonstrating actual energy savings in practice. The approach presented by Stoffel et al. (2022) first determines the number of BHEs n required to meet the buildings' energy demand. Next, it selects and subsequently activates the n hottest or coldest BHEs to meet the heating or cooling demand, respectively. The remaining BHEs are turned off, thus reducing the fluid volume to move in the field and allowing them to regenerate. BHE selection is achieved by applying a moving horizon estimator (MHE) to the monitoring data of the previous week, which estimates the temperature in all three discrete shells around the BHE (compare "Models and their parametrization" section). The MHE runs once per month, thus allowing to overcome one of the RC models' major shortcomings, its low long-term prediction accuracy, by continuous recalibration. To

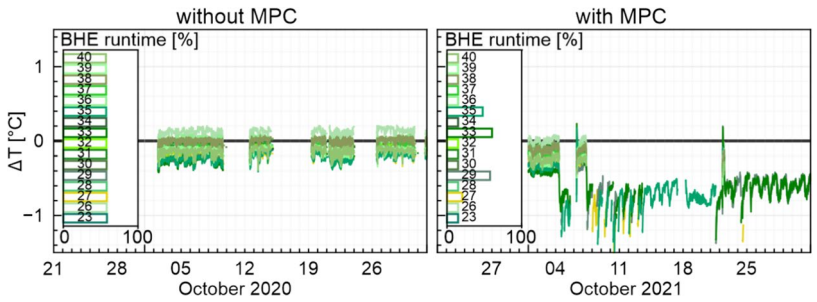

Fig. 8 Difference between the inlet and outlet temperatures of the BHEs of underground vault V3 (Fig. 1) without (left) and with (right) model predictive control using the RC model. The insets show the percentage runtime of the BHEs (numbered) for 31 days in October 2020 and October 2021, respectively

ensure turbulent flow in each BHE, dynamic hydraulic balancing is also applied. Because the hottest BHEs are used for heating and the coldest for cooling, both active and passive BHEs can regenerate. This improves the field's long-term performance, while the flow reduction reduces the power consumption of the hydraulic pumps.

This way, savings in electrical energy for the hydraulic pumps of 84% over 1 year were demonstrated. Figure 8 shows a comparison of the monitored temperature difference of BHEs in underground vault V3 without (October 2020) and with (October 2021) MPC. Without MPC, the temperature difference of all BHEs is close to zero, with a similar runtime of about 60% of the month for all BHEs. In difference, with MPC, only three BHEs are used majorly, which then have a higher temperature difference. The other BHEs run only 7% of the month, corresponding to the duration of the recalibration period. The BHE field's individually controllable valves are certainly a specialty in equipment that increases the investment cost of a BHE field's'. However, they allow to save energy when BHE fields are primarily used in part load.

Calibration to account for unknown load history

We motivated the model calibration for T_0 with the unknown operating history of the field. The calibration results showed that for short periods, the models yield different T_0. For example, in the summer period, T_0 was 13.11 °C, 12.77 °C and 13.7 °C for the g-function, hybrid, and RC models, respectively (Table 3). We concluded that the calibration reflects the cooling-dominated load history of the BHE field by a higher T_0. Subsequently, the 4-year calibration showed that the influence of the load history decreases with increasing calibration period, at least for the g-function and hybrid model.

Given the variability of T_0 depending on the chosen model and the duration of the calibration period, clarification regarding the definition of this temperature is necessary. The model formulations define the "undisturbed ground temperature" as an isotropic and homogeneous temperature at $t = 0$. However, in our BHE field, the temperature surrounding the boreholes is likely altered due to 10 years of operational history. Consequently, a temperature gradient from the fluid to the thermally undisturbed ground temperature develops, whose radius is influenced by the duration of the operation period and energy imbalances. Thus, simulating BHEs in an operational field means that the condition of the undisturbed ground temperature is not met. To avoid erroneous

fluid temperature predictions, two approaches are feasible: either, the operational history could be reconstructed, as demonstrated by Cupeiro Figueroa et al. (2021) using state observers. Alternatively, a less labor-intensive method might involve gathering sufficient monitoring data and calibrating the models for T_0. For short calibration periods, this temperature could then be interpreted as the "initial temperature around the BHE" rather than the "undisturbed ground temperature".

Obtaining the (really) undisturbed ground temperature by calibration may require long monitoring periods. Three months of monitoring data were required to determine the temperature yielding the best predictions in the g-function model. The hybrid model first showed a downward trend in the obtained T_0 before rising to a T_0 after 6 months (Fig. 6). This downward trend is attributed to the incorporation of the borehole heat capacity in the model formulation, known to elevate the outlet temperature (Shirazi and Bernier 2013). As previously concluded, it may be feasible to utilize the g-function model to estimate T_0 and subsequently employ it for calibrating the hybrid model. However, several constraints affect the applicability of these observations. The requisite calibration period likely depends on numerous factors, including the length of the operation history and the type of operation (clocked or continuous, balanced or unbalanced). Additionally, seasonal effects (heating/cooling) may influence calibration (Puttige et al. 2020a). Furthermore, the accurate selection of other subsurface properties (thermal conductivity, heat capacity) likely impacts the extent to which calibration enhances modeled temperature accuracy. If other model parameters deviate significantly from their true values, T_0 (as the sole calibration parameter) may compensate for this discrepancy, potentially compromising its physical significance. Consequently, the results of the assessment of the calibration period length cannot be generalized.

Problems related to operation characteristics

The results have shown that the operation strategy poses a challenge for the models. For example, all models exhibit their poorest agreement with measurement data during clocked operation, where the hydraulic pumps intermittently switch on and off. During off-times, the fluid temperature is affected by the ambient temperature in the control room (Yavuzturk and Spitler 2001) or ground (Naicker and Rees 2019), thus compromising the validity of the temperature measurements. Additionally, sensor uncertainty contributes to data quality issues. Gehlin et al. (2021) demonstrated that measurement errors for GSHP systems are more pronounced in systems with a low fluid temperature difference. Given the clocked operation and low temperature difference in the E.ON ERC field, the validity of comparing model results with measurement data is not always given.

Furthermore, these operational characteristics not only impact validation quality, but also GSHP efficiency. The low temperature difference suggests underutilization of the field's capacity, while on-off operation has been shown to degrade heat pump efficiency and longevity (Magraner et al. 2010; Waddicor et al. 2016). These observations align with findings from monitoring data of numerous other fields (e.g., Naicker 2015; Shirazi and Bernier 2022; Bockelmann and Fisch 2019) and highlight even more the necessity of flexible control algorithms such as MPC.

Summary and conclusions

The exploration of MPC algorithms offers the potential for increasing the energy efficiency of ground-source heat pump systems. Through validation against experimental data, our study has highlighted the strengths and limitations of four predictive models (a g-function, a resistance–capacitance, a hybrid, and a numerical model). We observed that the ground temperature is the most sensitive parameter of all models and that its precise calibration is crucial for accurate model performance. Our results show that the g-function model is suited for long-term simulations and strongly dependent on accurate calibration, which requires at least 3 months of monitoring data (to account for an unknown load history of 10 years). However, the g-function model can estimate the ground temperature most efficiently when the load history is unknown. This might be interesting when an already operating field gets equipped with sensors or control devices. In contrast, the RC model is well suited for short-term predictions, but similarly to the g-function model, requires calibration. The model's advantage is that each new timestep is only based on the previous timestep. Thus, it can easily be re-calibrated to achieve decent long-term predictions. Considering those simplifications, we have demonstrated how a g-function and RC model were used to optimize BHE field operation.

Overall, the hybrid model has the best performance in predicting the measured outlet temperature of a single BHE. The accuracy is similar to a fully 3-D numerical model, but the computation time 10^5 faster. Nonetheless, integrating the hybrid model in MPC would require a different and more complex implementation compared to the g-function and RC models. Even though not yet used in practice, our analysis suggests that the hybrid model combining the strengths of both the g-function and RC models could offer robust predictive capabilities across varying time scales, potentially advancing MPC strategies for GSHP systems.

Moreover, our findings highlight the broader implications of integrating MPC in ground-source heat pump systems. By maximizing energy savings and enhancing system performance, MPC strategies have the potential to address challenges such as infrequent heat pump operation and hydraulic pump cycling. As MPC strategies will be implemented in more practical settings, continuous monitoring and analysis will be essential for evaluating energy savings and, as a future work, assess the impact of model selection on energy savings. This way, the performance of the entire GSHP system, ground source and heat pump, together, will be increased.

Acknowledgements
We thank Lothar Ahrensmeier for his practical technical advice and his help in maintaining the temperature sensors in the BHE field.

Author contributions
EH, PS, SD, DK, AK: conceptualization, methodology, simulation, writing—original draft. EH: results evaluation and analysis, visualization, writing—original draft. NK: conceptualization, methodology, writing—review and editing, supervision, funding acquisition. DM: writing—review and editing, funding acquisition.

Funding
Open Access funding enabled and organized by Projekt DEAL. We are grateful for the funding by the Federal Ministry for Economic Affairs and Energy (BMWi), promotional reference 03ETW006A, and the funding provided by the BMBF BioökonomieREVIER funding scheme with its "BioRevierPlus" project, funding ID 031B1137EX.

Availability of data and materials
All data generated or analyzed during this study are available from the corresponding author on request.

Declarations

Competing interests
The authors declare that they have no conflict of interest.

Received: 2 April 2024 Accepted: 23 June 2024
Published online: 08 July 2024

References

384/6 S. SIA 384/6 Erdwärmesonden. SIA-Schweitzerischer Ingenieur und Architektenverein. 2021.
Andersson JAE, Gillis J, Horn G, Rawlings JB, Diehl M. CasADi: a software framework for nonlinear optimization and optimal control. Math Program Comput. 2019;11(1):1–36. https://doi.org/10.1007/s12532-018-0139-4.
Atam E, Helsen L. Ground-coupled heat pumps: part 1—literature review and research challenges in modeling and optimal control. Renew Sustain Energy Rev. 2016. https://doi.org/10.1016/J.RSER.2015.10.007.
Bauer D, Heidemann W, Müller-Steinhagen H, Diersch H-JG. Thermal resistance and capacity models for borehole heat exchangers. Int J Energy Res. 2011;35(4):312–20. https://doi.org/10.1002/er.1689.
Bayer P, de Paly M, Beck M. Strategic optimization of borehole heat exchanger field for seasonal geothermal heating and cooling. Appl Energy. 2014;136:445–53. https://doi.org/10.1016/j.apenergy.2014.09.029.
Bertagnolio S, Bernier M, Kummert M. Comparing vertical ground heat exchanger models. J Build Perform Simul. 2012;5(6):369–83. https://doi.org/10.1080/19401493.2011.652175.
Bockelmann F, Fisch MN. It works—long-term performance measurement and optimization of six ground source heat pump systems in Germany. Energies. 2019;12(24):4691. https://doi.org/10.3390/en12244691.
Cimmino M. The effects of borehole thermal resistances and fluid flow rate on the g-functions of geothermal bore fields. Int J Heat Mass Transf. 2015;91:1119–27. https://doi.org/10.1016/j.ijheatmasstransfer.2015.08.041.
Cimmino M. Fluid and borehole wall temperature profiles in vertical geothermal boreholes with multiple U-tubes. Renew Energy. 2016;96:137–47. https://doi.org/10.1016/j.renene.2016.04.067.
Cimmino M. Pygfunction: an open-source toolbox for the evaluation of thermal response factors for geothermal borehole fields. In: Proceedings of eSim 2018, the 10th conference of IBPSA-Canada. IBPSA Canada, Montréal, QC, Canada; 2018. p. 10.
Cimmino M. Semi-analytical method for g-function calculation of bore fields with series- and parallel-connected boreholes. Sci Technol Built Environ. 2019;25(8):1007–22. https://doi.org/10.1080/23744731.2019.1622937.
Cimmino M, Bernier M. A semi-analytical method to generate g-functions for geothermal bore fields. Int J Heat Mass Transf. 2014;70:641–50. https://doi.org/10.1016/j.ijheatmasstransfer.2013.11.037.
Claesson J, Hellström G. Multipole method to calculate borehole thermal resistances in a borehole heat exchanger. HVAC &R Res. 2011;17(6):895–911. https://doi.org/10.1080/10789669.2011.609927.
Cupeiro Figueroa I, Picard D, Helsen L. Short-term modeling of hybrid geothermal systems for model predictive control. Energy Build. 2020;215: 109884. https://doi.org/10.1016/j.enbuild.2020.109884.
Cupeiro Figueroa I, Cimmino M, Drgoňa J, Helsen L. Fluid temperature predictions of geothermal borefields using load estimations via state observers. J Build Perform Simul. 2021;14(1):1–19. https://doi.org/10.1080/19401493.2020.1838612.
de Wilde P. The gap between predicted and measured energy performance of buildings: a framework for investigation. Autom Constr. 2014;41:40–9. https://doi.org/10.1016/j.autcon.2014.02.009.
Dion G, Pasquier P, Marcotte D. Deconvolution of experimental thermal response test data to recover short-term g-function. Geothermics. 2022;100: 102302. https://doi.org/10.1016/j.geothermics.2021.102302.
Düber S, Ziegler M, Fuentes R. Development and validation of a computationally efficient hybrid model for temporal high-resolution simulations of geothermal bore fields. Int J Numer Anal Meth Geomech. 2022;46(14):2792–813. https://doi.org/10.1002/nag.3427.
Düber S, Fuentes R, Narsilio G. Exploiting heat gains along horizontal connection pipes in existing borehole heat exchanger fields. Geothermics. 2024;118: 102912. https://doi.org/10.1016/j.geothermics.2024.102912.
Eskilson P. Thermal analysis of heat extraction boreholes. Lund: Department of Mathematical Physics, University of Lund; 1987.
Fernández M, Eguía P, Granada E, Febrero L. Sensitivity analysis of a vertical geothermal heat exchanger dynamic simulation: calibration and error determination. Geothermics. 2017;70:249–59. https://doi.org/10.1016/j.geothermics.2017.06.012.
Fütterer J, Constantin A, Schmidt M, Streblow R, Müller D, Kosmatopoulos E. A multifunctional demonstration bench for advanced control research in buildings—monitoring, control, and interface system. In: IECON 2013—39th annual conference of the IEEE Industrial Electronics Society. Vienna: IEEE; 2013. p. 5696–701. https://doi.org/10.1109/IECON.2013.6700068.
Gehlin S. Thermal response test: method development and evaluation; 2002.
Gehlin S, Spitler JD, Berglöf K, Pallard WM, Witte H. IEA HPT Annex 52—long-term performance monitoring of GSHP systems for commercial, institutional and multi-family buildings. Technical report, Heat Pump Centre; 2021. https://doi.org/10.23697/M2EM-XQ83.
Heim E, Pasquier P, Dion G, Stoffel P, Klitzsch N. Reconstruction of experimental thermal response functions from monitoring data of a borehole heat exchanger field. In: IGSHPA research conference, Polytechnique Montreal; 2024. https://doi.org/10.22488/okstate.24.000018
Hellström G. Ground heat storage: thermal analyses of duct storage systems. Lund: Lund University; 1991.
Herman J, Usher W. SALib: an open-source python library for sensitivity analysis. J Open Source Softw. 2017;2(9):97. https://doi.org/10.21105/joss.00097.

Iwanaga T, Usher W, Herman J. Toward SALib 2.0: advancing the accessibility and interpretability of global sensitivity analyses. Socio-Environ Syst Model. 2022;4:18155. https://doi.org/10.18174/sesmo.18155.
Keller J, Rath V, Bruckmann J, Mottaghy D, Clauser C, Wolf A, Seidler R, Bücker HM, Klitzsch N. SHEMAT-suite: an open-source code for simulating flow, heat and species transport in porous media. SoftwareX. 2020;12: 100533. https://doi.org/10.1016/j.softx.2020.100533.
Kümpel A, Stoffel P, Müller D. Development of a long-term operational optimization model for a building energy system supplied by a geothermal field. J Therm Sci. 2022. https://doi.org/10.1007/s11630-022-1616-7.
Li M, Li P, Chan V, Lai ACK. Full-scale temperature response function (G-function) for heat transfer by borehole ground heat exchangers (GHEs) from sub-hour to decades. Appl Energy. 2014;136:197–205. https://doi.org/10.1016/j.apenergy.2014.09.013.
Liu J, Wang F, Gao Y, Zhang Y, Cai W, Wang M, Wang Z. Influencing factors analysis and operation optimization for the long-term performance of medium-deep borehole heat exchanger coupled ground source heat pump system. Energy Build. 2020;226: 110385. https://doi.org/10.1016/j.enbuild.2020.110385.
Lund JW, Toth AN. Direct utilization of geothermal energy 2020 worldwide review. Geothermics. 2021;90: 101915. https://doi.org/10.1016/j.geothermics.2020.101915.
Luo J, Zhao H, Jia J, Xiang W, Rohn J, Blum P. Study on operation management of borehole heat exchangers for a large-scale hybrid ground source heat pump system in China. Energy. 2017;123:340–52. https://doi.org/10.1016/j.energy.2017.01.136.
Ma Z, Xia L, Gong X, Kokogiannakis G, Wang S, Zhou X. Recent advances and development in optimal design and control of ground source heat pump systems. Renew Sustain Energy Rev. 2020;131: 110001. https://doi.org/10.1016/j.rser.2020.110001.
Magraner T, Montero Á, Quilis S, Urchueguía JF. Comparison between design and actual energy performance of a HVAC-ground coupled heat pump system in cooling and heating operation. Energy Build. 2010;42(9):1394–401. https://doi.org/10.1016/j.enbuild.2010.03.008.
Marcotte D, Pasquier P. Fast fluid and ground temperature computation for geothermal ground-loop heat exchanger systems. Geothermics. 2008;37(6):651–65. https://doi.org/10.1016/j.geothermics.2008.08.003.
Mitchell MS, Spitler JD. An enhanced vertical ground heat exchanger model for whole-building energy simulation. Energies. 2020;13(16):4058. https://doi.org/10.3390/en13164058.
Mottaghy D, Dijkshoorn L. Implementing an effective finite difference formulation for borehole heat exchangers into a heat and mass transport code. Renew Energy. 2012;45:59–71. https://doi.org/10.1016/j.renene.2012.02.013.
Naicker SS. Performance analysis of a large-scale ground source heat pump system. PhD thesis, Unpublished, Leicester, UK; 2015.
Naicker SS, Rees SJ. Long-term high frequency monitoring of a large borehole heat exchanger array. Renew Energy. 2019;145:1528–42. https://doi.org/10.1016/j.renene.2019.07.008.
Nash JE, Sutcliffe JV. River flow forecasting through conceptual models part I—a discussion of principles. J Hydrol. 1970;10(3):282–90.
Paly M, Hecht-Méndez J, Beck M, Blum P, Zell A, Bayer P. Optimization of energy extraction for closed shallow geothermal systems using linear programming. Geothermics. 2012;43:57–65. https://doi.org/10.1016/j.geothermics.2012.03.001.
Pasquier P, Marcotte D. Short-term simulation of ground heat exchanger with an improved TRCM. Renew Energy. 2012;46:92–9. https://doi.org/10.1016/j.renene.2012.03.014.
Pasquier P, Zarrella A, Labib R. Application of artificial neural networks to near-instant construction of short-term g-functions. Appl Therm Eng. 2018;143:910–21. https://doi.org/10.1016/j.applthermaleng.2018.07.137.
Puttige AR, Andersson S, Östin R, Olofsson T. Improvement of borehole heat exchanger model performance by calibration using measured data. J Build Perform Simul. 2020a;13(4):430–42. https://doi.org/10.1080/19401493.2020.1761451.
Puttige AR, Andersson S, Östin R, Olofsson T. A novel analytical-ANN hybrid model for borehole heat exchanger. Energies. 2020b;13(23):6213. https://doi.org/10.3390/en13236213.
Puttige AR, Andersson S, Östin R, Olofsson T. Modeling and optimization of hybrid ground source heat pump with district heating and cooling. Energy Build. 2022;264: 112065. https://doi.org/10.1016/j.enbuild.2022.112065.
Rawlings JB, Mayne DQ, Diehl M. Model predictive control: theory, computation, and design. 2nd ed. Madison: Nob Hill Publishing; 2017.
Saltelli A. Making best use of model evaluations to compute sensitivity indices. Comput Phys Commun. 2002;145(2):280–97. https://doi.org/10.1016/S0010-4655(02)00280-1.
Saltelli A, Annoni P, Azzini I, Campolongo F, Ratto M, Tarantola S. Variance based sensitivity analysis of model output. Design and estimator for the total sensitivity index. Comput Phys Commun. 2010;181(2):259–70. https://doi.org/10.1016/j.cpc.2009.09.018.
Shirazi AS, Bernier M. Thermal capacity effects in borehole ground heat exchangers. Energy Build. 2013;67:352–64. https://doi.org/10.1016/j.enbuild.2013.08.023.
Soltan Mohammadi H, Ringel LM, de Paly M, Bayer P. Sequential long-term optimization of shallow geothermal systems under descriptive uncertainty and dynamic variation of heating demand. Geothermics. 2024;121: 103021. https://doi.org/10.1016/j.geothermics.2024.103021.
Spitler JD. Addressing the building energy performance gap with measurements. Sci Technol Built Environ. 2020;26(3):283–4. https://doi.org/10.1080/23744731.2020.1718871.
Spitler JD, Gehlin SEA. Long-term GSHP system performance measurement in the USA and Europe. 2022. https://doi.org/10.22488/okstate.22.000012.
Stoffel P, Kümpel A, Müller D. Cloud-based optimal control of individual borehole heat exchangers in a geothermal field. J Therm Sci. 2022. https://doi.org/10.1007/s11630-022-1639-0.
VDI 4640: VDI 4640 Blatt 2 - Thermische Nutzung des Untergrunds - Erdgekoppelte Wärmepumpenanlagen. VDI-Gesellschaft Energie und Umwelt; 2019.
Verhelst C, Helsen L, D'haeseleer W. Model predictive control of ground coupled heat pump systems in office buildings (Modelgebaseerde regeling van grondgekoppelde warmtepompsystemen in kantoorgebouwen). 2012.

Virtanen P, Gommers R, Oliphant TE, Haberland M, Reddy T, Cournapeau D, Burovski E, Peterson P, Weckesser W, Bright J, van der Walt SJ, Brett M, Wilson J, Millman KJ, Mayorov N, Nelson ARJ, Jones E, Kern R, Larson E, Carey CJ, Polat İ, Feng Y, Moore EW, VanderPlas J, Laxalde D, Perktold J, Cimrman R, Henriksen I, Quintero EA, Harris CR, Archibald AM, Ribeiro AH, Pedregosa F, van Mulbregt P. SciPy 1.0 contributors: SciPy 1.0: fundamental algorithms for scientific computing in python. Nat Methods. 2020;17:261–72. https://doi.org/10.1038/s41592-019-0686-2.

Waddicor DA, Fuentes E, Azar M, Salom J. Partial load efficiency degradation of a water-to-water heat pump under fixed set-point control. Appl Therm Eng. 2016;106:275–85. https://doi.org/10.1016/j.applthermaleng.2016.05.193.

Wetter M, Huber A. Vertical borehole heat exchanger EWS model. TRNSYS type. 1997;451.

Witte HJL, Cazorla-Marín A, Corberan J. An efficient borehole heat exchanger model for the analysis of transient thermal response: comparison with some existing models. 2018.

Yang H, Cui P, Fang Z. Vertical-borehole ground-coupled heat pumps: a review of models and systems. Appl Energy. 2010;87(1):16–27. https://doi.org/10.1016/j.apenergy.2009.04.038.

Yavuzturk C, Spitler JD. Field validation of a short time step model for vertical ground-loop heat exchangers. In: ASHRAE Transactions, vol. 107, PART. 1. 2001. p. 617–25.

Zarrella A, Scarpa M, De Carli M. Short time step analysis of vertical ground-coupled heat exchangers: the approach of CaRM. Renew Energy. 2011;36(9):2357–67. https://doi.org/10.1016/j.renene.2011.01.032.

Zhan S, Chong A. Data requirements and performance evaluation of model predictive control in buildings: a modeling perspective. Renew Sustain Energy Rev. 2021;142: 110835. https://doi.org/10.1016/j.rser.2021.110835.

Zhang X, Han Z, Ji Q, Zhang H, Li X. Thermal response tests for the identification of soil thermal parameters: a review. Renew Energy. 2021;173:1123–35. https://doi.org/10.1016/j.renene.2020.12.028.

Publisher's Note